ACS MATERIALS Au
AN OPEN ACCESS JOURNAL OF THE AMERICAN CHEMICAL SOCIETY
pubs.acs.org/materialsau Article

Atomic-Scale Modification of Oxidation Phenomena on the Ge(100) Surface by Si Alloying

Mikhail Kuzmin,* Juha-Pekka Lehtiö, Zahra Jahanshah Rad, Svetlana V. Sorokina, Marko P. J. Punkkinen, Hannu-Pekka Hedman, Risto Punkkinen, Pekka Laukkanen, and Kalevi Kokko

Cite This: https://doi.org/10.1021/acsmaterialsau.1c00039 Read Online

ACCESS | Metrics & More | Article Recommendations | Supporting Information

Downloaded via UNIV OF TURKU on February 10, 2022 at 10:00:52 (UTC).
See https://pubs.acs.org/sharingguidelines for options on how to legitimately share published articles.

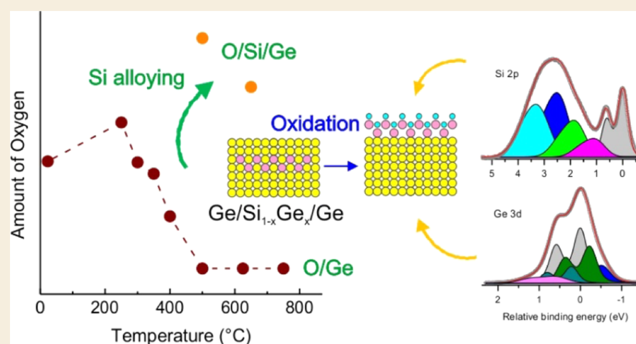

ABSTRACT: Properties of Ge oxides are significantly different from those of widely used Si oxides. For example, the instability of GeO_x at device junctions causes electronic defect levels that degrade the performance of Ge-containing devices (e.g., transistors and infrared detectors). Therefore, the passivating Si layers have been commonly used at Ge interfaces to reduce the effects of Ge oxide instability and mimic the successful strategy of Si oxidation. To contribute to the atomic-scale knowledge and control of oxidation of such Si-alloyed Ge interfaces (O/Si/Ge), we present a synchrotron radiation core-level study of O/Si/Ge, which is combined with scanning probe microscopy measurements. The oxidation processes and electronic properties of O/Si/Ge(100) are examined as functions of Si amount and oxidation doses. In particular, the incorporation of Si into Ge is shown to cause the strengthening of Ge−O bonds and the increase of incorporated oxygen amount in oxide/Ge junctions, supporting that the method is useful to decrease the defect-level densities.

KEYWORDS: *interface, atomic and electronic structure, alloying, passivation, photoelectron spectroscopy, germanium, oxide*

1. INTRODUCTION

Since the invention of a bipolar junction transistor containing a block of germanium in 1947,[1] Ge-based applications have firmly carved out a niche in the semiconductor industry.[2−10] For instance, owing to a higher electron and especially hole mobility in Ge relative to that in Si (3900 and 1900 $cm^2/(V·s)$ versus 1400 and 500 $cm^2/(V·s)$, respectively), utilizing germanium as a channel material in metal-oxide-semiconductor field-effect transistors (MOSFETs) holds promise in future nanoscale devices. Furthermore, its band gap of 0.7 eV makes Ge useful material for infrared photodiodes integrated with Si technology, for example, to develop photonic integrated circuits. The weakness of the Ge material, however, is related to poor electrical properties and solubility of Ge oxides.[1,2,11,12] One main problem is that Ge oxides are not enough stable; they start to decompose at device interfaces even at 300 °C or lower temperatures.[13] On the other hand, it is difficult to avoid the interaction of Ge surfaces with oxygen during device processing. Therefore, some Ge oxides can anyway form at device interfaces (e.g., Al_2O_3/Ge or HfO_2/Ge). The device structures need to be postannealed typically at 300°C or higher temperatures (e.g., postmetallization annealing), causing the decomposition of unintentional interfacial Ge oxides and uncontrolled changes in the interface structure. To overcome these difficulties, one of the most studied solutions is interposing a passivating Si layer between a high-k film and a Ge substrate, leading to improved electrical properties of the resulting dielectric/Ge stack.[14−17] For this reason, much attention has been paid to the high-k/SiO_2/Ge junctions.[2,3]

Despite the successful implementation of the passivating Si layer at the high-k/Ge interface, the atomic-level understanding of such structures is still far from being complete. Also, the effects of Si overlayers on Ge oxidation are debated. Furthermore, it is known that some drawbacks can arise as a result of Ge passivation with Si. For example, increasing the thickness of the Si layer can cause a decrease of carrier population in the higher-mobility Ge channel, and therefore, the Si layer thickness requires precise optimization.[18−21] Furthermore, physical realization of highly crystalline Si/Ge(100) interfaces is a nontrivial issue since the formation mechanism of strained Si/Ge(100) interfaces is governed by two opposite processes involving mass transport via the interface, namely, (i) Si indiffusion into the substrate and (ii) Ge segregation on top of the Si/Ge sample, leading to the formation of a buried $Si_{1-x}Ge_x$ alloy layer below the uppermost

Received: August 24, 2021
Revised: December 5, 2021
Accepted: December 8, 2021

© XXXX The Authors. Published by American Chemical Society

Ge (2 × 1)-reconstructed layer.[22] Thus, the passivation of the Ge(100) substrate by Si atoms is actually not straightforward, and the oxidation mechanism for the Si-modified Ge(100) surface is not well understood yet.

In this work, we have combined a set of complementary experimental techniques, including high-resolution core-level (CL) photoelectron spectroscopy using synchrotron radiation, X-ray photoelectron spectroscopy (XPS), low-energy electron diffraction (LEED), scanning tunneling microscopy (STM), and scanning tunneling spectroscopy (STS) to probe the structural and electronic properties of O−Si−Ge(100) systems as functions of the deposited Si amount and oxygen dose. In particular, such properties can be significantly changed by even small amounts of incorporated oxygen atoms, which can be identified by high-resolution synchrotron radiation photoemission facilities. Indeed, synchrotron-based experiments have been performed more and more for semiconductor interfaces.[23−26] We demonstrate that proper Si alloying of Ge surfaces combined with preoxidation of SiGe is a potential method to develop Ge device interfaces.

2. EXPERIMENTAL DETAILS

The CL measurements were carried out *in situ* at beamline I4 at the MAX-lab synchrotron radiation facility in Lund, Sweden. The CL spectra were acquired with a SPECS Phoibos 100 analyzer with an acceptance angle of ±1° at room temperature (RT). The instrumental resolution was better than 100 meV. The photon energy ($h\nu$) and emission angle (θ_e) were varied for optimizing the probing depth. The binding energy was determined by a reference Ta sample in good contact with the Ge samples. The Ge 3d and Si 2p spectra were quantitatively analyzed by a standard fitting procedure described elsewhere.[27] The O 1s spectra could not be taken because of the limited range of $h\nu$ (≤200 eV) at the beamline.

The STM, STS, and XPS measurements were performed *in situ* in a separate multichamber, ultrahigh vacuum (UHV) system with a base pressure below 1×10^{-10} mbar. It was equipped with an Omicron STM operating at RT, a nonmonochromatic Mg Kα (1253.6 eV) X-ray source, four-grid LEED optics, and Ar^+ ion bombardment facilities. The STM images were taken with W tips in the constant-current mode. The STS measurements were performed over the well-defined area of sample surfaces in the grid mode, i.e., at every fourth point along every fourth scanning line of the topography image. The tunneling current (I)−sample bias voltage (V) curves were averaged, numerically differentiated, and finally plotted in the form of $(dI/dV)/(I/V)$ (normalized differential conductivity)−V. As demonstrated earlier,[28,29] the $(dI/dV)/(I/V)-V$ curves reflect the local density of state (LDOS) distributions of probed surfaces above (at the positive bias polarity, $V > 0$) and below (at the negative bias polarity, $V < 0$) the Fermi energy ($V = 0$). The WSXM package[30] was partly utilized for processing the STM data.

The clean Ge(100) surfaces (n-type, Sb doped, ∼1×10^{18} to 1×10^{19} cm^{-3}) were prepared by several cycles of Ar^+ ion bombardment at 400 °C and subsequent annealing at 630 °C until sharp (2 × 1) patterns were observed by LEED. Also, the cleanness of Ge(100) surfaces was verified by STM and Ge 3d CL spectroscopy. The Si deposition was performed from an evaporator with a silicon rod heated by passing direct current through it. The evaporator was carefully outgassed prior to the Si deposition. The deposition rate was calibrated by observing the attenuation of Ge 3d photoemission signal from the test Ge samples covered progressively by Si layers at RT as well as by estimating the ratio of covered and bare surface areas in STM images of Si(111)(7 × 7) with submonolayer quantities of Si atoms adsorbed at RT. One monolayer (ML) of Si atoms on Ge(100) was referred to as the atomic concentration of 6.24×10^{14} cm^{-2}, which is equal to the number of Ge atoms on the clean surface. The substrate was kept at RT during Si deposition, followed by annealing the sample at 500 °C for 30 min. This leads to well-defined epitaxial Si/Ge structures with long-range order.[22] Oxidation was performed at an O_2 pressure of 2×10^{-7} Torr. The oxygen doses are expressed in Langmuir (1 L = 1×10^{-6} Torr × 1 s) throughout.

3. RESULTS AND DISCUSSION

3.1. Oxygen Bond Formation

As shown earlier,[22] the number of nonequivalent Si and Ge bonding sites at Si/Ge(100) interfaces strongly depends on the number of deposited silicon atoms. Therefore, we separately describe oxidation of interfaces with different nominal Si amounts, namely, 1 and 4 ML (hereafter Si_{1ML}/Ge and Si_{4ML}/Ge, respectively). The former structure can be considered as a model substrate for growing improved oxide films on Ge(100) since the Si atoms, which control the oxidation process in such junctions, have a single bonding site and form a well-defined crystalline buried $Si_{1-x}Ge_x$ alloy layer at Si_{1ML}/Ge.[22] In the latter structure, the Si atoms have several bonding sites, illustrating the complexity of O−Si−Ge systems. The Si_{1ML}/Ge and Si_{4ML}/Ge structures were oxidized at 300 °C with various O_2 doses.

3.1.1. Epitaxial Si_{1ML}/Ge. High-resolution CL spectroscopy using synchrotron radiation is a powerful tool to probe the structural arrangement of Si/Ge junctions since this technique can easily distinguish the Si and Ge atoms, in contrast to LEED and STM. As known, this technique is aimed at identifying surface- or/and interface-related core-level shifts (CLSs) that derive from the nonequivalence of surface/interface atoms as compared to the bulk.[31] The CLSs bring information about the bonding sites and charge states of individual atoms at both surface and subsurface regions. Furthermore, synchrotron radiation allows one to vary the probing depth of the sample by optimizing the photon energy. In addition, the variation of the emission angle can efficiently change the surface and bulk sensitivity of CL spectra. The enhanced surface sensitivity is particularly relevant here because a very small amount of atoms (<10^{12} cm^{-2}) can cause significant electrical losses.

Figure 1 shows the Ge 3d and Si 2p CL spectra along with their fittings for the Si_{1ML}/Ge prior to oxidation. The Ge 3d

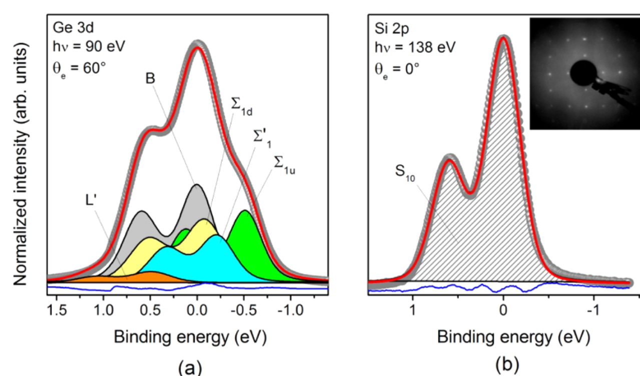

Figure 1. (a) Ge 3d and (b) Si 2p spectra and their deconvolution results for Si_{1ML}/Ge. The experimental conditions ($h\nu$, θ_e) are (90 eV, 60°) and (138 eV, 0°), respectively. Inset: LEED pattern from the Si_{1ML}/Ge surface; the electron energy is 128 eV.

spectrum is taken at $h\nu$ = 90 eV, which corresponds to the kinetic energy of photoelectrons around 57 eV and grazing emission angle (θ_e = 60°) for the enhancement of surface sensitivity. The raw data are depicted by gray circles and obtained after background correction by the Shirley method

and normalization to the spectral maximum. Spectral deconvolution was performed by a standard least-squares fitting procedure using a linear combination of spin−orbit Voigt functions. The minimum number of components (i.e., spin−orbit doublets) needed to fit the spectrum adequately was always used. The Lorentzian width (0.150 eV), spin−orbit splitting (0.594 eV), and branching ratio (0.667 ± 10%) were constrained for all Ge 3d components. The CLSs, their relative intensities, and Gaussian widths (GWs) were variable parameters. The wavy line below the fitted spectrum illustrates the residual acquired as a difference between the data and fit curve.

As the surface of Si_{1ML}/Ge is terminated by Ge atoms arranging the well-known (2×1) reconstruction (the corresponding LEED pattern is presented in the inset of Figure 1),[22] the Ge 3d spectrum should include individual components originating from different Ge atoms of this reconstruction, namely, the upper and lower atoms of buckled Ge dimers in the topmost layer as well as the second-layer Ge atoms. Indeed, our analysis indicates that the Ge 3d line shape in Figure 1a is composed of five spin−orbit components (depicted by filled doublets), among which Σ_{1u}, Σ_{1d}, and Σ'_1 are very similar to the respective components for the clean Ge(100)(2 × 1) surface,[27] that is, the components related to the dimer-up and dimer-down atoms of the topmost layer as well as Ge atoms in the second layer, respectively. The CLSs of Σ_{1u}, Σ_{1d}, and Σ'_1 relative to the binding energy of bulk component B (set to 0 eV) and their relative intensities are presented in Table 1.

Yet, the fitting scheme with the three surface components, Σ_{1u}, Σ_{1d}, and Σ'_1, cannot reproduce well the higher-binding-energy tail of the Ge 3d line shape for Si_{1ML}/Ge. The reasonable fitting requires the introduction of an extra small component (labeled L′ in Figure 1a) on the higher-binding-energy side of the bulk emission. This component does not derive from the regular (2 × 1) structure but stems from surface defects.[27] Thus, the fitting scheme for the Ge 3d spectrum in Figure 1a is identical to that of the clean Ge(100) surface,[27] and no additional components are required to decompose this line shape. The intensity ratio of the bulk (B) and surface-shifted (Σ_{1u}, Σ_{1d}, Σ'_1, and L′) components in Figure 1a is 1:2. Their GWs lie in between 0.33 and 0.41 eV, which are slightly higher than the GWs of the clean surface.[22] This broadening appears to be quite natural because of the incorporation of Si atoms into the Ge host, leading to additional strain in the substrate lattice and a higher degree of local disorder of the Ge structure. The close similarity of Ge 3d line shapes for Si_{1ML}/Ge and clean Ge also suggests that the former includes at least the uppermost two layers of Ge atoms, similar to the pristine, Si-free, surface.

The Si 2p spectrum of Si_{1ML}/Ge in Figure 1b is acquired at $h\nu$ = 138 eV, i.e., the kinetic energy of photoelectrons of around 34 eV, and θ_e = 0°. The striking feature of this spectrum is that it is composed of a single spin−orbit doublet, which is labeled S_{10}. This means that all Si atoms incorporated in the host lattice are equivalent, i.e., there is only a single type of site for the incorporated Si atoms. They occupy Ge-lattice sites,[22] giving rise to the high homogeneity and good crystallinity of the buried $Si_{1-x}Ge_x$ layer. Most likely, such behavior facilitates the crystallinity of the top of the resulting structure terminated by segregated Ge atoms, forming the native (2 × 1) reconstruction. That is, the Si 2p and Ge 3d line shapes in Figure 1 are fully consistent with the well-defined epitaxial Ge-(2 × 1)/$Si_{1-x}Ge_x$/Ge(100) arrangement in the case of the Si_{1ML}/Ge stack.

Oxidation of Si_{1ML}/Ge was done at three O_2 doses, i.e., 10, 25, and 100 L at 300 °C. The resulting structures will be denoted O_{10L}/Si_{1ML}/Ge, O_{25L}/Si_{1ML}/Ge, and O_{100L}/Si_{1ML}/Ge hereafter. No long-range order is found for such structures by LEED and STM (not shown here). It is known that both clean Ge(100) and Si(100) surfaces can be readily oxidized at the above temperature.[32−35] For this reason, one may expect, on the one hand, that the oxygen atoms are bonded to both Ge and Si species at O/Si_{1ML}/Ge junctions. On the other hand, the top of the Si_{1ML}/Ge substrate is terminated by 2 MLs of Ge atoms, whereas the Si atoms locate beneath, as remarked above. Hence, one could tentatively expect that the bonding of oxygen to Ge rather than Si is more feasible. The CLS measurements can shed light on the bonding details in oxidized Si_{1ML}/Ge structures. First, oxidation of Si/Ge structures causes significant changes of Si 2p and Ge 3d line shapes, leading to pronounced features on the higher-binding-energy side of spectra (Figure S1). Figures 2 and 3 present the Si 2p and Ge 3d spectra taken for O_{10L}/Si_{1ML}/Ge, O_{25L}/Si_{1ML}/Ge, and O_{100L}/Si_{1ML}/Ge at θ_e = 0 and 60°, respectively. As seen, the Si 2p line shape (Figure 2) is drastically dependent on the oxygen dose. Even without any fitting, one can easily resolve a broad feature on the higher-binding-energy side of S_{10}. Upon increasing the oxygen dose, this feature becomes more prominent, while the intensity of S_{10} decreases systematically. The fitting reveals that the broad feature comprises four spin−orbit components, S_{11}, S_{12}, S_{13}, and S_{14}, at all O_2 doses used. These components are broadened and respectively shifted by ∼1.02, 1.76, 2.42, and 3.15 eV relative to S_{10}. Such shifts are a reminiscence of those of SiO_2/Si(100) interfaces, where there are four oxidation states for the Si

Table 1. Fitting Parameters for the Decomposed Ge 3d and Si 2p Spectra from Si_{1ML}/Ge in Figure 1 and O/Si_{1ML}/Ge in Figures 2 and 3[a]

Si_{1ML}/Ge	O_{10L}/Si_{1ML}/Ge	O_{25L}/Si_{1ML}/Ge	O_{100L}/Si_{1ML}/Ge
Ge 3d [θ_e = 60°]			
			(B) 0 [0.29]
(B) 0 [0.33]	(B) 0 [0.39]	(B) 0 [0.39]	(Σ_{11}) −0.52 [0.07]
(Σ_{1u}) −0.51 [0.23]	(Σ_{11}) −0.51 [0.20]	(Σ_{11}) −0.51 [0.15]	(Σ_{12}) −0.23 [0.15]
(Σ'_1) −0.21 [0.16]	(Σ_{12}) −0.23 [0.22]	(Σ_{12}) −0.22 [0.27]	(Σ_{13}) 0.19 [0.18]
(Σ_{1d}) −0.08 [0.23]	(Σ_{13}) 0.21 [0.19]	(Σ_{13}) 0.22 [0.12]	(Σ_{15}) 1.14 [0.11]
(L′) 0.49 [0.04]		(Σ_{14}) 0.60 [0.07]	(Σ_{16}) 1.59 [0.07]
			(Σ_{17}) 2.61 [0.13]
Si 2p {θ_e = 0°} [θ_e = 60°]			
(S_{10}) 0 {1}	(S_{10}) 0 {0.50} [0.35]	(S_{10}) 0 {0.20} [0.12]	(S_{10}) 0 {0.08} [0.08]
	(S_{11}) 1.05 {0.15} [0.11]	(S_{11}) 1.02 {0.08} [0.04]	(S_{11}) 1.00 {0.03} [<0.01]
	(S_{12}) 1.73 {0.19} [0.22]	(S_{12}) 1.78 {0.17} [0.15]	(S_{12}) 1.78 {0.16} [0.11]
	(S_{13}) 2.44 {0.08} [0.20]	(S_{13}) 2.40 {0.29} [0.38]	(S_{13}) 2.43 {0.41} [0.52]
	(S_{14}) 3.13 {0.08} [0.12]	(S_{14}) 3.18 {0.26} [0.31]	(S_{14}) 3.13 {0.32} [0.29]

[a]The individual spectral components are presented in parentheses. The CLSs are given in eV. The relative intensities are given in brackets for the case of θ_e = 60° and braces for θ_e = 0°. See the text for more details.

https://doi.org/10.1021/acsmaterialsau.1c00039
ACS Mater. Au XXXX, XXX, XXX−XXX

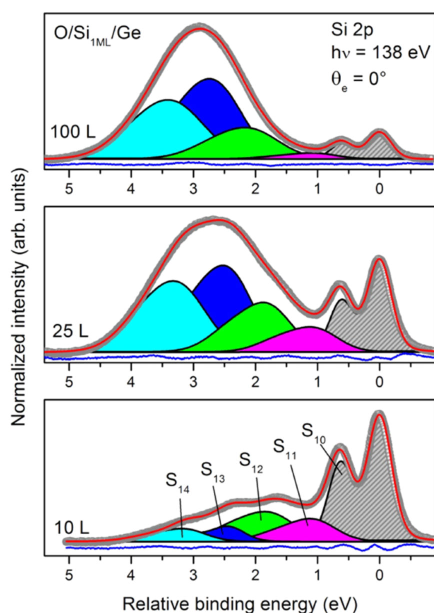

Figure 2. Si 2p spectra and fitting results for O/Si_{1ML}/Ge structures grown with various oxygen doses. The photon energy is 138 eV. The emission angle is 0°. The O_2 doses are 10, 25, and 100 L.

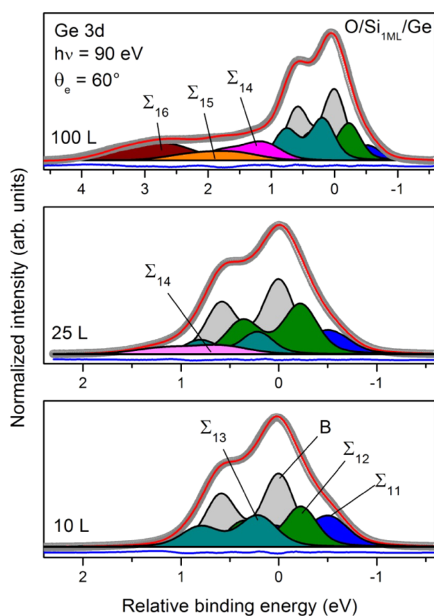

Figure 3. Ge 3d spectra and fitting results for O/Si_{1ML}/Ge structures grown with various oxygen doses. The photon energy is 90 eV. The emission angle is 60°. The O_2 doses are 10, 25, and 100 L.

species and their CLSs are 0.99 eV (Si^{1+}), 1.85 eV (Si^{2+}), 2.65 eV (Si^{3+}), and 3.68 eV (Si^{4+}).[32,33] Based on this similarity, we conclude that the Si atoms readily interact with O atoms at the Si_{1ML}/Ge interface, leading to four Si (sub)oxide phases. It is interesting that a one-to-one correspondence of CLSs in the two systems, O/Si(100) and O/Si_{1ML}/Ge(100), is incomplete, and the observed difference of CLSs systematically increases with the number of the oxidation state. This infers that within the initial-state model, the electron charge transferred from the Si atom to the O atom is slightly smaller at the O/Si/Ge interface than that at the O/Si one. Most likely, this is because Si/Ge, due to the difference in electronegativity of Si (1.9) and Ge (2.0), has a small degree of ionicity, in contrast to purely covalent Si crystals, and therefore, the Si atoms act as cations in the alloy phase and the electron charge transferred from such atoms to O atoms is slightly less than the respective charge at the SiO_x/Si interface.

More information about the oxide phases at the O/Si_{1ML}/Ge(100) interfaces can be obtained from the analysis of the relative intensities of Si 2p components. Intensities of individual components are presented for the cases of θ_e = 0 and 60°, i.e., in more bulk- and more surface-sensitive conditions, respectively, in Table 1. (A comparison of raw Si 2p spectra from Si_{1ML}/Ge(100) and O/Si_{1ML}/Ge(100) in more bulk- and more surface-sensitive conditions can be found in Figure S2.) Neglecting the photoelectron diffraction and attenuation effects in multilayer structures, it is assumed that the intensity ratios of these components roughly reflect the number ratios of respective atoms. On this basis, a few conclusions can be made from the data in Table 1. First, the oxygen dose systematically affects the number ratio of Si atoms, which are bonded and not bonded to O atoms. In particular, the intensity ratio of S_{10} and (S_{11} + S_{12} + S_{13} + S_{14}) is 1:1 at 10 L, 1:4 at 25 L, and ∼1:12 at 100 L in the more bulk-sensitive condition and respectively ∼1:2, ∼1:7, and ∼1:12 in the more surface-sensitive one. This means that the dose as large as 100 L is not enough to oxidize the silicon dopant entirely at Si_{1ML}/Ge(100).

Second, the evolution of Si oxide stoichiometry with the O_2 dose is complicated. The fractions of Si species with various oxidation states (0, 1+, 2+, 3+, and 4+) versus oxygen dose at θ_e = 0° are presented in Figure 4. At 10 L, the dominating

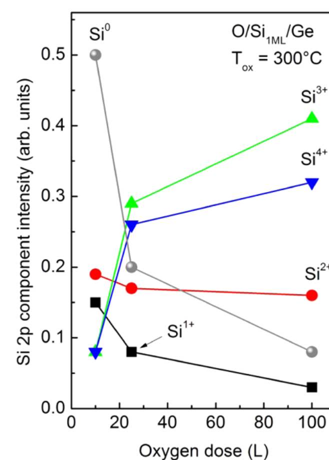

Figure 4. Intensities of Si 2p components originating from Si^0, Si^{1+}, Si^{2+}, Si^{3+}, and Si^{4+} species at oxidized Si1ML/Ge interfaces as a function of the oxygen dose.

species are Si^{2+}, while Si^{3+} and Si^{4+} are rather rare; the total intensity of these two components is about that of Si^{1+}. The structure of the oxide layer has changed with the dose. The fractions of Si^{3+} and Si^{4+} have increased, whereas that of Si^{1+} has decreased. The fraction of Si^{2+} decreases slightly with the dose too. In general, such behavior is caused by that the Si atoms become more and more surrounded by O atoms upon increasing the exposure to oxygen. The Si^{3+} species have still remained dominating at both 25 and 100 L.

Third, the question of where the Si (sub)oxides are located at the stack can be addressed on the basis of the data in Table 1. Tentatively, two possible scenarios can be considered for the

https://doi.org/10.1021/acsmaterialsau.1c00039
ACS Mater. Au XXXX, XXX, XXX−XXX

Si_{1ML}/Ge oxidation process. One could expect the O atoms to diffuse into the $Si_{1-x}Ge_x$ alloy layer below the uppermost Ge(2 × 1) reconstruction and form the oxide phases mixed with $Si_{1-x}Ge_x$. Alternatively, the Si atoms may outdiffuse, and therefore, the oxide phases form above the alloy layer. To elucidate the oxidation mechanism, the normal-emission Si 2p spectra in Figure 2 were compared with those acquired at θ_e = 60° (not shown here). The relative intensities of Si 2p components at the two emission angles are presented in Table 1. It is clearly seen that S_{10} and S_{11} are clearly more bulk-sensitive, whereas S_{13} and S_{14} are more surface-sensitive. This means that Si oxide phases are mostly located above the $Si_{1-x}Ge_x$ alloy layer. This is the case especially for the Si^{3+} and Si^{4+} species, i.e., Si_2O_3 and SiO_2 phases. The exception is the Si^{1+} species (Si_2O) that are located near the alloy layer.

Figure 3 shows the Ge 3d spectra for O_{10L}/Si_{1ML}/Ge, O_{25L}/Si_{1ML}/Ge, and O_{100L}/Si_{1ML}/Ge. Surprisingly, these spectra indicate that interface oxidation has a selective character. At 10 L, the Ge 3d spectrum includes three interface-related components, of which CLSs are −0.51 (Σ_{11}), −0.23 (Σ_{12}), and 0.21 eV (Σ_{13}) relative to the bulk. It is well known that oxidation of the Ge(100) shifts the Ge 3d emission, depending on the oxidation state, by 0.7−4.0 eV toward the higher binding energy relative to the bulk.[34,36−44] Therefore, Σ_{11}, Σ_{12}, and Σ_{13} cannot be attributed to Ge atoms bonded to oxygen. In other words, the O atoms interact with the Si atoms and do not with the Ge atoms at 10 L. Furthermore, Σ_{11}, Σ_{12}, and Σ_{13} cannot be assigned to the Ge-(2 × 1) reconstruction either. Therefore, the top of Si_{1ML}/Ge is rearranged after oxidation, which is clearly supported by the lack of long-range order in LEED and STM. Obviously, the removal of (2×1) reconstruction is caused by the formation of SiO_x phases.

Upon increasing the oxidation dose, extra interface-related components, in addition to Σ_{11}, Σ_{12}, and Σ_{13}, appear in Ge 3d spectra of Figure 3. A Σ_{14} component is found at 25 L and Σ_{15}, Σ_{16}, and Σ_{17} ones at 100 L. The extra components are significantly shifted toward the higher binding energy relative to the bulk emission (see in Table 1). The CLS of Σ_{14} (0.60 eV) is close to that of Ge^{1+} species at the GeO_x/Ge(100) interfaces.[34−42] Based on the relative intensity of this component, the number of respective Ge atoms is ∼0.2 ML. Therefore, we assume that the Ge structure at O/Si_{1ML}/Ge becomes slightly oxidized at 25 L. The Σ_{14} component can be also contributed by the grain boundary Ge atoms[22] because an increase in O or/and Si mass transport through the topmost Ge structure can stimulate the formation of such defects.

The interpretation of Σ_{15} (1.14 eV), Σ_{16} (1.59 eV), and Σ_{17} (2.61 eV) is more straightforward. These components can be assigned to Ge atoms with 1+, 2+, and 3+ oxidation states, respectively. The total amount of such atoms is ∼2/3 ML. Thus, oxidation of the Ge structure at O/Si_{1ML}/Ge is significantly enhanced at 100 L, while the Ge substrate has still remained nonoxidized at 10 L. This difference can be also supported well by a comparison of difference spectra for O/Si_{1ML}/Ge and Si_{1ML}/Ge at 10 and 100 L (Figure S3).

3.1.2. Epitaxial Si_{4ML}/Ge. Oxidation of Si_{4ML}/Ge is performed at 300 °C and the O_2 doses of 25, 100, and 500 L (hereafter O_{25L}/Si_{4ML}/Ge, O_{100L}/Si_{4ML}/Ge, and O_{500L}/Si_{4ML}/Ge, respectively). Figures 5 and 6 present the Ge 3d and Si 2p spectra and their fittings for such structures along with the nonoxidized Si_{4ML}/Ge substrate for comparison. The Ge 3d spectra are taken at the experimental conditions (hν, θ_e) = (90 eV, 60°), and the Si 2p spectra are taken at (hν, θ_e) = (138 eV, 0°). Table 2 shows the CLSs and relative intensities of individual components for these spectra. Also, results obtained at (hν, θ_e) = (90 eV, 0°) and (138 eV, 60°) are included for comparison.

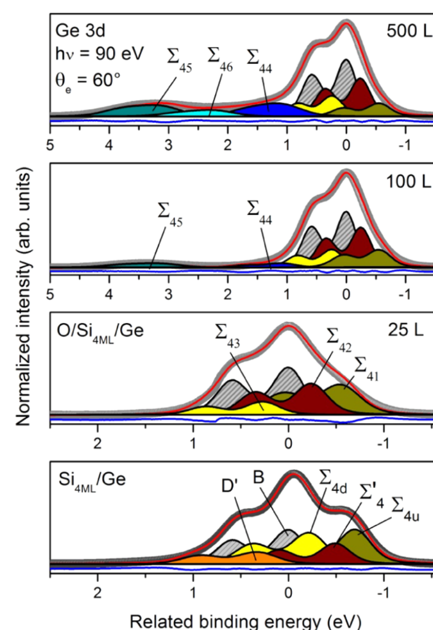

Figure 5. Ge 3d spectra and fitting results for the Si_{4ML}/Ge and O/Si_{4ML}/Ge interfaces. The photon energy is 90 eV. The emission angle is 60°. The O_2 doses are 25, 100, and 500 L.

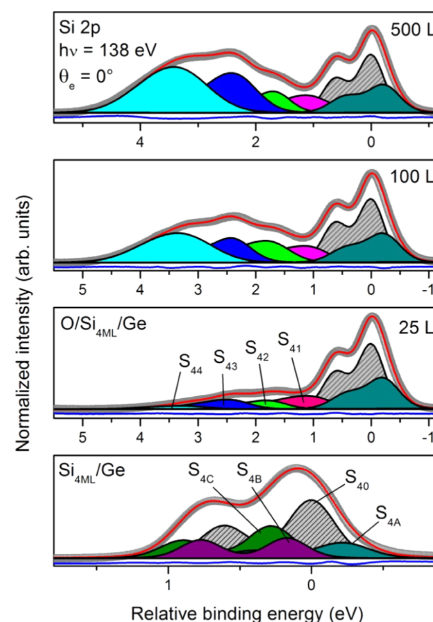

Figure 6. Si 2p spectra and fitting results for the Si_{4ML}/Ge and O/Si_{4ML}/Ge interfaces. The photon energy is 138 eV. The emission angle is 0°. The O_2 doses are 25, 100, and 500 L.

For the nonoxidized interface, four Ge 3d components (Σ_{4u}, Σ_{4d}, Σ_4', and D′) are identified in addition to the bulk one. Their interpretation has been elsewhere.[22] Comparing the intensities of these components at the two emission angles (see Table 2 and Figure S3), the former three are clearly surface-sensitive. The Σ_{4u} and Σ_{4d} are due to the dimer-up and dimer-down Ge atoms in the topmost atomic layer and the Σ_4' to the second-layer Ge atoms. These components are the fingerprint

https://doi.org/10.1021/acsmaterialsau.1c00039
ACS Mater. Au XXXX, XXX, XXX−XXX

Table 2. Fitting Parameters for the Decomposed Ge 3d and Si 2p Spectra from Si_{4ML}/Ge and O/Si_{4ML}/Ge in Figures 5 and 6[a]

Si_{4ML}/Ge	O_{25L}/Si_{4ML}/Ge	O_{100L}/Si_{4ML}/Ge	O_{500L}/Si_{4ML}/Ge
	Ge 3d {θ_e = 0°} [θ_e = 60°]		
		(B) 0 [0.37]	(B) 0 [0.32]
(B) 0 {0.31} [0.23]	(B) 0 {0.55} [0.36]	(Σ_{41}) −0.56 [0.14]	(Σ_{41}) −0.55 [0.08]
(Σ_{4u}) −0.65 {0.17} [0.24]	(Σ_{41}) −0.54 {0.12} [0.28]	(Σ_{42}) −0.25 [0.27]	(Σ_{42}) −0.24 [0.21]
(Σ'_4) −0.42 {0.13} [0.16]	(Σ_{42}) −0.24 {0.16} [0.25]	(Σ_{43}) 0.24 [0.13]	(Σ_{43}) 0.24 [0.12]
(Σ_{4d}) −0.15 {0.17} [0.24]	(Σ_{43}) 0.26 {0.17} [0.11]	(Σ_{44}) 1.08 [0.04]	(Σ_{44}) 1.07 [0.11]
(D′) 0.21 {0.22} [0.13]		(Σ_{45}) 3.13 [0.05]	(Σ_{46}) 2.22 [0.06]
			(Σ_{45}) 3.13 [0.10]
	Si 2p {θ_e = 0°} [θ_e = 60°]		
	(S_{40}) 0 {0.44}	(S_{40}) 0 {0.27}	(S_{40}) 0 {0.21}
(S_{4C}) 0.28 {0.25} [0.28]	(S_{4A}) −0.21 {0.25}	(S_{4A}) −0.21 {0.16}	(S_{4A}) −0.22 {0.12}
(S_{4B}) 0.17 {0.14} [0.28]	(S_{41}) 1.02 {0.12}	(S_{41}) 1.05 {0.09}	(S_{41}) 1.05 {0.09}
(S_{40}) 0 {0.47} [0.33]	(S_{42}) 1.76 {0.07}	(S_{42}) 1.74 {0.13}	(S_{42}) 1.68 {0.09}
(S_{4A}) −0.21 {0.14} [0.11]	(S_{43}) 2.44 {0.09}	(S_{43}) 2.40 {0.14}	(S_{43}) 2.33 {0.21}
	(S_{44}) 3.19 {0.03}	(S_{44}) 3.17 {0.21}	(S_{44}) 3.24 {0.28}

[a]The individual spectral components are presented in parentheses. The CLSs are given in eV. The relative intensities are given in brackets for θ_e = 60° and braces for θ_e = 0°. See the text for more details.

of Ge(2 × 1) reconstruction which has been confirmed by STM and LEED.[22] In contrast, the D′ is bulk-sensitive and can be assigned to the grain boundary atoms.

The Si 2p spectrum of the nonoxidized Si_{4ML}/Ge reveals four components, as shown in Figure 6. Among them, the most bulk-sensitive one is S_{40} (Table 2). Its binding energy is set to 0 eV. The S_{4B} and S_{4C} components are surface-sensitive and shifted by 0.17 and 0.28 eV relative to S_{40}. The S_{4A} component is bulk-sensitive and shifted by −0.21 eV relative to S_{40}. All of these originate from Si sites in the $Si_{1-x}Ge_x$ alloy layer below the Ge-terminated (2 × 1) surface.

When Si_{4ML}/Ge is oxidized, the surface-sensitive S_{4B} and S_{4C} have disappeared. Instead, four extra components, S_{41}, S_{42}, S_{43}, and S_{44} should be introduced to reproduce the higher-binding-energy side of Si 2p spectra in Figure 6. It is seen from Tables 1 and 2 that S_{41}, S_{42}, S_{43}, and S_{44} are similar to S_{11}, S_{12}, S_{13}, and S_{14} for O/Si_{1ML}/Ge. Hence, we conclude that S_{41}, S_{42}, S_{43}, and S_{44} stem from the Si^{1+}−Si^{4+} species in oxide phases. It is also seen from Table 2 that the intensity ratio of (S_{40} + S_{4A}):(S_{41} + S_{42} + S_{43} + S_{44}), i.e., the number ratio of Si atoms, which are bonded and not bonded to O atoms, changes systematically with the O_2 dose. It is ~2:1 at 25 L, ~3:4 at 100 L, and ~1:2 at 500 L. The changes of fractions of Si^{1+}−Si^{4+} species at O/Si_{4ML}/Ge with the oxygen dose are shown in Figure 7. The lowest oxidation state is dominating at 25 L, while the highest oxidation state is the most prominent at 100 and 500 L.

The changes of Ge 3d line shape upon oxidation of Si_{4ML}/Ge are similar to those of Si_{1ML}/Ge. At 25 ML, the Ge (2 × 1) reconstruction on top of the interface is destroyed, and Σ_{41}, Σ_{42}, and Σ_{43} components have appeared (Table 2). They

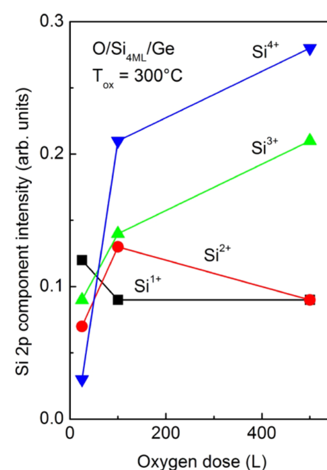

Figure 7. Intensities of Si 2p components originating from Si^0, Si^{1+}, Si^{2+}, Si^{3+}, and Si^{4+} species at oxidized Si_{4ML}/Ge interfaces as a function of the oxygen dose.

clearly resemble Σ_{11}, Σ_{12}, and Σ_{13} in Table 1. Σ_{41} and Σ_{42} are more surface-sensitive, and Σ_{43} is more bulk-sensitive. No oxidation of Ge and oxide-related Ge 3d components is found at 25 L. Thus, similar to the case of Si_{1ML}/Ge, selective oxidation of Si_{4ML}/Ge occurs at lower O_2 doses.

It is also seen from Figure 5 and Table 2 that oxide-related Ge 3d components appear with increasing the O_2 dose. At 100 L, Σ_{44} and Σ_{45} are required to reproduce the higher-binding-energy tail of the spectrum. The former can be assigned to the Ge^{1+} species, and the latter can be assigned to the Ge^{3+} or/and Ge^{4+} ones. At 500 L, a component Σ_{46} is added eventually. It originates from the Ge^{2+} or/and Ge^{3+} species. Interestingly, the number of O-bonded Ge sites increases mostly at the expense of the Ge atoms, which are the origin of Σ_{41}. This means that the Ge oxide phases are located on the surface of the O/Si_{4ML}/Ge stack.

The above results indicate that Si alloying is a promising method to stabilize or strengthen Ge oxides. Si alloying facilitates the formation of higher oxidation states of Ge atoms, such as 3+ and 4+. For comparison, only the 1+ and 2+ oxidation states are found for GeO_x/Ge(100) at similar conditions.[35] This infers that Si can facilitate the strengthening of Ge−O bonds.

3.2. Comparison of Oxide/Ge Interfaces with and without Modification by Si Alloying

As shown in the preceding sections, the Ge substrates modified by Si alloying have a selective character of oxidation, where Si atoms tend to readily interact with oxygen. At the same time, Si alloying can increase the stability of Ge−O bonds. To investigate further this technologically relevant issue, we compared oxidation of clean Ge(100) and Si/Ge(100) at different temperatures. To produce the Si-alloyed Ge(100) substrate, the optimization of several parameters was needed. As shown in Section 3.1, the thickness of the oxide phase increases with the number of incorporated Si atoms. On the other hand, the quality of the Ge/$Si_{1-x}Ge_x$/Ge stack and homogeneity of the alloy layer are also affected by the Si amount. Earlier, it has been shown that the deposition of Si atoms on Ge(100) by portions (one portion is 1 ML), followed by annealing the substrate, allowed us to fabricate high-quality junctions.[22] Here, we used this method for growing the Si-alloyed Ge substrate. Four portions of Si

https://doi.org/10.1021/acsmaterialsau.1c00039
ACS Mater. Au XXXX, XXX, XXX−XXX

atoms (1 ML each) were deposited on clean Ge(100) at RT. After the deposition of each portion, the sample was annealed at 500 °C. As a result, the Ge-(2 × 1)/$Si_{4\times1ML}$/Ge(100) structure with the (2 × 1) reconstruction on the top was obtained. An STM image of such a structure is presented in Figure 8. It shows that the surface morphology has high quality

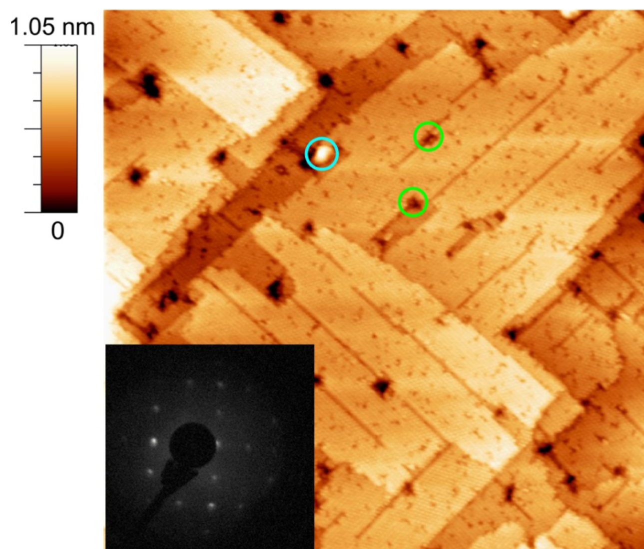

Figure 8. STM image and LEED pattern (inset) from $Si_{4\times1ML}$/Ge. The bias voltage (V) is 2.0 V. The tunneling current (I_t) is 0.10 nA. The scanning area is 100 × 100 nm^2. The local dark and bright areas are outlined by circles (for details, see the text). The electron energy is 131 eV.

and that the structure possesses an epitaxial character. Interestingly, the STM image also reveals very local dark and bright areas outlined by circles. Such defects resemble those of the clean Ge(100) surface cleaned by ion sputtering.[45] In the inset, a LEED pattern from this surface is presented. It clearly shows the (2 × 1) periodicity.

A difference in oxidation of $Si_{4\times1ML}$/Ge and clean Ge substrates (the O_2 dose 200 L) at various temperatures is illustrated in Figure 9. The measure of oxygen amount at O_{200L}/$Si_{4\times1ML}$/Ge and O_{200L}/Ge was the intensity of the O 1s peak acquired with XPS (shown on the vertical axis of Figure 9). It is seen that clean Ge can be efficiently oxidized in the

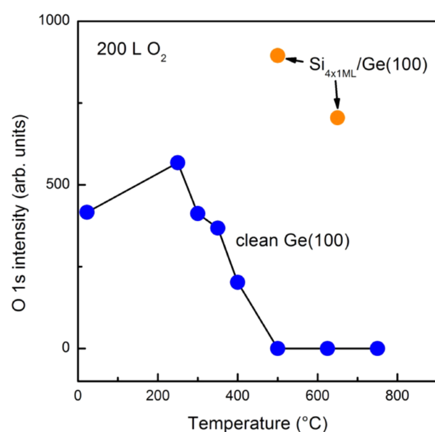

Figure 9. O 1s intensity measured by XPS for O_{200L}/Ge and O_{200L}/$Si_{4\times1ML}$/Ge structures as a function of the oxidation temperature.

range from RT to 400 °C. At 500 °C and higher, no oxygen is found, and the Ge substrate has remained nonoxidized at all. It means that the Ge oxide phases formed on clean Ge(100) are completely unstable at ≥500 °C. In contrast, $Si_{4\times1ML}$/Ge(100) can be readily oxidized at both 500 and 650 °C, with the O amount being ∼1.5 to 2.0 times higher than that of the clean Ge(100).

The differences of O_{200L}/$Si_{4\times1ML}$/Ge(100) and O_{200L}/Ge(100) in structural and electronic properties have been studied by STM and STS. Although the practical applications often contain an insulator film deposited still on the top of Si/Ge or Ge, these applications also contain oxidized Si/Ge or Ge at the interfaces. Thus, STM and STS can provide interesting information about these interface parts existing in applications. Figure 10 presents the STM images for the $Si_{4\times1ML}$/Ge(100), O_{200L}/$Si_{4\times1ML}$/Ge(100), and O_{200L}/Ge(100) surfaces. It is seen that $Si_{4\times1ML}$/Ge(100) is highly ordered and that patterning occurs due to the incorporation of 4 ML Si. Upon oxidation, the long-range order has reduced on both surfaces according to LEED, but it can be still seen in Figure 10b a trace of the initial 2D terrace-step structure after the oxidation of $Si_{4\times1ML}$/Ge(100).

The analysis of morphologies of these surfaces was performed by roughness distributions obtained from STM data in Figure 10. This approach is described in more detail in the literature.[22,46] The distributions of tip heights acquired in measuring the STM images (filled circles) are shown in Figure 11. It is seen that each curve can be fitted with a single Gaussian peak. The single component used in the fitting can infer that the surface phase is homogeneous. This means that the surface is covered with the oxide phase entirely. However, the width of distributions is not the same. In the case of O_{200L}/Ge(100), it is significantly broadened. The standard deviation is 0.945 nm for this surface, while it is 0.137 nm for both $Si_{4\times1ML}$/Ge(100) and O_{200L}/$Si_{4\times1ML}$/Ge(100). The smoothness and 2D terrace-step structure of O_{200L}/$Si_{4\times1ML}$/Ge(100) as compared to those of O_{200L}/Ge(100) suggest a higher crystalline order for the O_{200L}/$Si_{4\times1ML}$/Ge(100) sample. Indeed, LEED shows both 1 × 1 and 2 × 1 spots for this sample (see the inset of Figure 11b), while no LEED spots are found for O_{200L}/Ge(100). Higher crystallinity typically suggests a lower density of point defects at the Ge interface.

Figure 12 presents the $(dI/dV)/(I/V)$ spectra measured for clean Ge, $Si_{4\times1ML}$/Ge, O_{200L}/$Si_{4\times1ML}$/Ge, and O_{200L}/Ge by STS. As already remarked (Section 2), such spectra reflect the LDOS of probed surfaces. It is seen that the clean Ge and $Si_{4\times1ML}$/Ge surfaces are semiconducting and have the tunneling gap (or band gap) characteristic for the p-type-like sample (i.e., the Fermi level is close to the VB maximum). When these surfaces are oxidized, the surface electronic structure is drastically modified. The LDOS near the Fermi level (see the inset) is observed to be essentially larger for O_{200L}/Ge than that for O_{200L}/$Si_{4\times1ML}$/Ge. This implies a higher density of defect levels in the band gap for the O_{200L}/Ge interface. This result is well consistent with the STM results in Figures 10 and 11. Moreover, the above difference in LDOS in the band gaps of O_{200L}/Ge and O_{200L}/$Si_{4\times1ML}$/Ge interfaces fully agrees with a comparison of capacitance−voltage and leakage current measurements for two capacitors fabricated on the basis of these interfaces (Figure S4). Thus, the presented approach, where a crystalline Si/Ge surface is intentionally oxidized in a controlled way before an insulator film growth, has the potential to develop Ge-based devices. In the

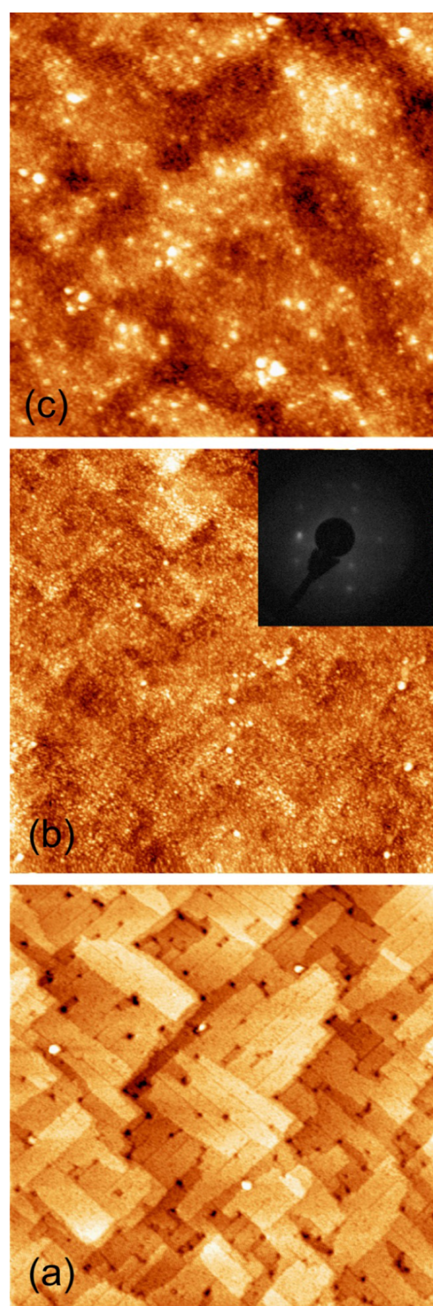

Figure 10. STM images for (a) $Si_{4\times1ML}$/Ge, (b) O_{200L}/$Si_{4\times1ML}$/Ge, and (c) O_{200L}/Ge structures. The bias voltage (V) is 2.0 V. The tunneling current (I_t) is 0.10 nA. The scanning area is 200 × 200 nm^2. The inset in (b) shows a LEED pattern from O_{200L}/$Si_{4\times1ML}$/Ge. The electron energy is 133 eV.

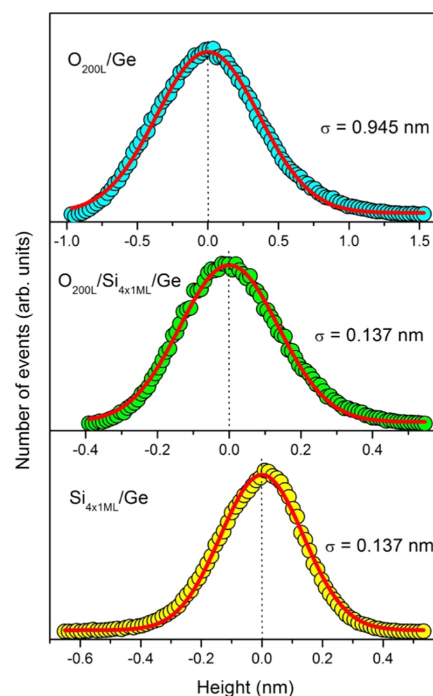

Figure 11. Roughness distributions for STM images in Figure 10.

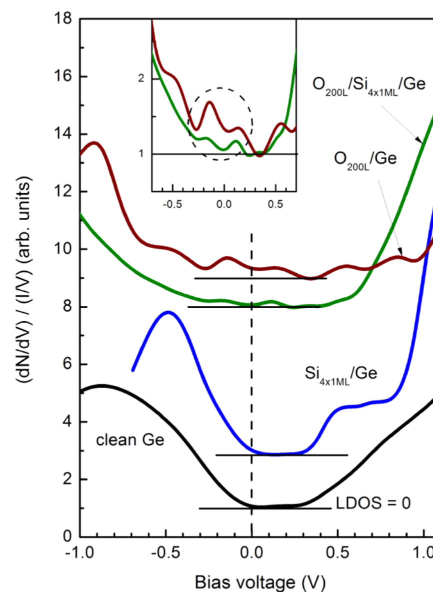

Figure 12. $(dI/dV)/(I/V)$ spectra for the clean Ge, $Si_{4\times1ML}$/Ge, O_{200L}/$Si_{4\times1ML}$/Ge, and O_{200L}/Ge surfaces measured by STS. These spectra represent the LDOS of the probed samples. The inset shows a comparison of spectra near the Fermi level in more detail.

commonly used Si passivation method, the deposited Si layer is not oxidized beforehand, but it is worth noting that the Si-containing surface becomes finally oxidized at some stage(s) of the device processing.

3.3. Stabilization of Ge–O Bonds via Si Alloying

Finally, we examine the changes in Ge–O bonding when the Ge substrate is modified by Si alloying. To this end, Ge 3d spectra were taken by XPS for the O_{200L}/Ge(100) and O_{200L}/$Si_{4\times1ML}$/Ge(100) structures along with the clean Ge surface. Figure 13 illustrates the comparison of the spectrum of each of the oxidized structures with that of the clean substrate (note that spectral fragments that are affected by oxidation are mostly shown). It is seen that for O_{200L}/Ge(100) at 300 °C oxidation, the higher-binding-energy features related to the Ge atoms bonded to O atoms are shifted mostly by ∼0.9 to 2.2 eV relative to the bulk. These XPS features are not high in intensity but are still significant. Therefore, two main oxide-related Ge species have oxidation states of 1+ and 2+. For O_{200L}/$Si_{4\times1ML}$/Ge(100) oxidized at 500 °C, such features are mostly shifted by ∼2 to 3 and ∼3.7 to 3.8 eV, meaning that the most frequent oxide-related Ge species have higher oxidation states. Therefore, the incorporation of Si at the Ge interface allows one to replace lower oxidation states with higher ones

https://doi.org/10.1021/acsmaterialsau.1c00039
ACS Mater. Au XXXX, XXX, XXX−XXX

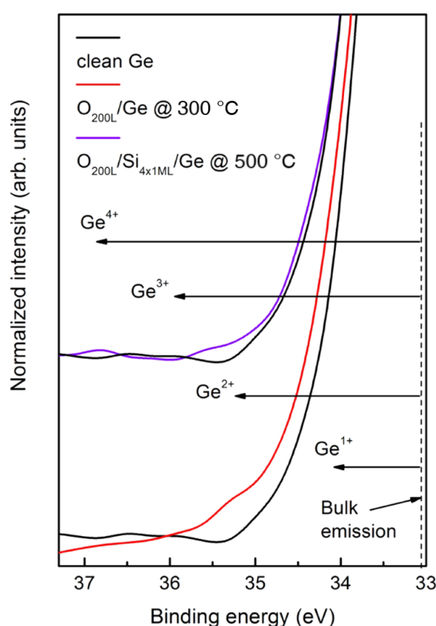

Figure 13. Comparison of Ge 3d peaks measured by XPS for the clean Ge, O_{200L}/Ge (the oxidation temperature is 300 °C), and $O_{200L}/Si_{4\times1ML}$/Ge (500 °C).

for Ge atoms. It is believed that the higher Ge oxides are more stable. Thus, Si alloying leads to the strengthening of Ge−O bonds and more stable Ge oxides at the dielectric/Ge junctions.

4. CONCLUSIONS

Combining synchrotron radiation photoelectron spectroscopy, STM, STS, LEED, and XPS measurements, we have studied the oxidation processes and effects at the well-defined Si/Ge interfaces. It has been shown that oxidation of Si-alloyed Ge surfaces is strongly dependent on the silicon amount and has a selective character: at low oxygen doses (i.e., 10 L at 300 °C), Si−O bonds are formed solely, while no Ge−O bond is found. Four oxidation states of Si atoms are identified at such interfaces, and it is shown that the ratio of Si oxidation states is dependent on the oxygen dose. At higher O_2 doses, the formation of Ge−O bonds occurs in addition to Si−O ones. Based on the above results, the preparation of the Si-alloyed Ge substrate is optimized for further oxidation, and the differences in stability and structural, electronic, and electrical properties of $O_{200L}/Si_{4\times1ML}$/Ge(100) and O_{200L}/Ge(100) are examined. It has been shown that the oxide films are completely unstable on clean Ge at 500 °C and higher, while $Si_{4\times1ML}$/Ge(100) can be readily oxidized at 500−650 °C, with the O amount being ∼1.5 to 2.0 times higher with respect to the case of the clean Ge(100) substrate. That is, the Ge substrate modified by Si alloying can be oxidized more efficiently than the clean Ge(100) substrate. It is also shown that the above Si passivation method leads to the strengthening of Ge−O bonds on the Ge(100) surface and is useful to decrease the defect state density at Ge-based device interfaces.

■ ASSOCIATED CONTENT

Supporting Information

The Supporting Information is available free of charge at https://pubs.acs.org/doi/10.1021/acsmaterialsau.1c00039.

Evolution of Ge 3d and Si 2p spectral line shapes of Si_{1ML}/Ge and Si_{4ML}/Ge interfaces upon oxidation, comparison of Si 2p spectra taken for the O/Si_{1ML}/Ge structures at more bulk-sensitive and more surface-sensitive conditions, Ge 3d difference spectra for O/Si_{1ML}/Ge and Si_{1ML}/Ge at various oxygen doses, and *C*−*V* and leakage current curves for capacitors with Ge and Si-alloyed Ge substrates (PDF)

■ AUTHOR INFORMATION

Corresponding Author

Mikhail Kuzmin − *Department of Physics and Astronomy, University of Turku, FI-20014 Turku, Finland; Ioffe Institute, Russian Academy of Sciences, St. Petersburg 194021, Russian Federation;* orcid.org/0000-0002-0138-9850; Email: m.kuzmin@mail.ioffe.ru

Authors

Juha-Pekka Lehtiö − *Department of Physics and Astronomy, University of Turku, FI-20014 Turku, Finland*
Zahra Jahanshah Rad − *Department of Physics and Astronomy, University of Turku, FI-20014 Turku, Finland*
Svetlana V. Sorokina − *Ioffe Institute, Russian Academy of Sciences, St. Petersburg 194021, Russian Federation*
Marko P. J. Punkkinen − *Department of Physics and Astronomy, University of Turku, FI-20014 Turku, Finland*
Hannu-Pekka Hedman − *Department of Information Technology, University of Turku, FI-20014 Turku, Finland*
Risto Punkkinen − *Department of Information Technology, University of Turku, FI-20014 Turku, Finland*
Pekka Laukkanen − *Department of Physics and Astronomy, University of Turku, FI-20014 Turku, Finland;* orcid.org/0000-0003-4220-985X
Kalevi Kokko − *Department of Physics and Astronomy, University of Turku, FI-20014 Turku, Finland*

Complete contact information is available at: https://pubs.acs.org/10.1021/acsmaterialsau.1c00039

Notes

The authors declare no competing financial interest.

■ ACKNOWLEDGMENTS

The authors are grateful to the MAX-lab staff for their assistance. Support of the Academy of Finland (via project 296469) and Business Finland TUTLI (via project SISUPRO-CO 1671/31/2018) is also acknowledged.

■ REFERENCES

(1) Bardeen, J.; Brattain, W. H. The Transistor, A Semi-Conductor Triode. *Phys. Rev.* **1948**, *74*, No. 230.
(2) Wallace, R. M.; McIntyre, P. C.; Kim, J.; Nishi, Y. Atomic Layer Deposition of Dielectrics on Ge and III−V Materials for Ultrahigh Performance Transistors. *MRS Bull.* **2009**, *34*, 493−503.
(3) Kamata, Y. High-k/Ge MOSFETs for future nanoelectronics. *Mater. Today* **2008**, *11*, 30−38.
(4) Liu, C.; Ma, W.; Chen, M.; Ren, W.; Sun, D. A vertical silicon-graphene-germanium transistor. *Nat. Commun.* **2019**, *10*, No. 4873.
(5) Zheng, X.; Zhang, M.; Shi, X.; Wang, G.; Zheng, L.; Yu, Y.; Huang, A.; Chu, P. K.; Gao, H.; Ren, W.; Di, Z.; Wang, X. Fluorinated Graphene in Interface Engineering of Ge-Based Nanoelectronics. *Adv. Funct. Mater.* **2015**, *25*, 1805−1813.
(6) Vines, P.; Kuzmenko, K.; Kirdoda, J.; Dumas, D. C. S.; Mirza, M. M.; Millar, R. W.; Paul, D. J.; Buller, G. S. High performance planar

germanium-on-silicon single-photon avalanche diode detectors. *Nat. Commun.* **2019**, *10*, No. 1086.
(7) Arimura, H.; Cott, D.; Boccardi, G.; Loo, R.; Wostyn, K.; Witters, L.; Conard, T.; Suhard, S.; van Dorp, D.; Dekkers, H.; Ragnarsson, L.-Å.; Mitard, J.; De Heyn, V.; Mocuta, D.; Collaert, N.; Horiguchi, N. Record Gm_{SAT}/SS_{SAT} and PBTI Reliability in Si-Passivated Ge nFinFETs by Improved Gate-Stack Surface Preparation. *IEEE Trans. Electron Devices* **2019**, *66*, 5387−5392.
(8) Sammak, A.; Sabbagh, D.; Hendrickx, N. W.; Lodari, M.; Wuetz, B. P.; Tosato, A.; Yeoh, L.; Bollani, M.; Virgilio, M.; Schubert, M. A.; Zaumseil, P.; Capellini, G.; Veldhorst, M.; Scappucci, G. Shallow and Undoped Germanium Quantum Wells: A Playground for Spin and Hybrid Quantum Technology. *Adv. Funct. Mater.* **2019**, *29*, No. 1807613.
(9) Virot, L.; Crozat, P.; Fédéli, J.-M.; Hartmann, J.-M.; Marris-Morini, D.; Cassan, E.; Boeuf, F.; Vivien, L. Germanium avalanche receiver for low power interconnects. *Nat. Commun.* **2014**, *5*, No. 4957.
(10) Hendrickx, N. W.; Lawrie, W. I. L.; Russ, M.; van Riggelen, F.; de Snoo, S. L.; Schouten, R. N.; Sammak, A.; Scappucci, G.; Veldhorst, M. A four-qubit germanium quantum processor. *Nature* **2021**, *591*, 580.
(11) Sardashti, K.; Hu, K.-T.; Tang, K.; Park, S.; Kim, H.; Madisetti, S.; McIntyre, P.; Oktyabrsky, S.; Siddiqui, S.; Sahu, B.; Yoshida, N.; Kachian, J.; Kummel, A. Sulfur passivation for the formation of Si-terminated Al_2O_3/SiGe(001) interfaces. *Appl. Surf. Sci.* **2016**, *366*, 455−463.
(12) Lee, T.-E.; Ke, M.; Toprasertpong, K.; Takenaka, M.; Takagi, S. Reduction of MOS Interface Defects in $TiN/Y_2O_3/Si_{0.78}Ge_{0.22}$ Structures by Trimethylaluminum Treatment. *IEEE Trans. Electron Devices* **2020**, *67*, 4067−4072.
(13) Kato, K.; Taoka, N.; Sakashita, M.; Nakatsuka, O.; Zaima, S. Oxygen and germanium migration at low temperature influenced by the thermodynamic nature of the materials used in germanium metal-insulator-semiconductor structures. *Appl. Phys. Lett.* **2015**, *107*, No. 102102.
(14) Nicholas, G.; Grasby, T. J.; Fulgoni, D. J. F.; Beer, C. S.; Parsons, J.; Meuris, M.; Heyns, M. M. High Mobility Strained Ge pMOSFETs With High-κ/Metal Gate. *IEEE Electron Device Lett.* **2007**, *28*, 825−827.
(15) Vitkavage, D. J.; Fountain, G. G.; Rudder, R. A.; Hattangady, S. V.; Markunas, R. J. Gating of germanium surfaces using pseudomorphic silicon interlayers. *Appl. Phys. Lett.* **1988**, *53*, 692−694.
(16) Bai, W. P.; Lu, N.; Kwong, D.-L. Si Interlayer Passivation on Germanium MOS Capacitors With High-*k* Dielectric and Metal Gate. *IEEE Electron Device Lett.* **2005**, *26*, 378−380.
(17) Houssa, M.; Chagarov, E.; Kummel, A. Surface Defects and Passivation of Ge and III−V Interfaces. *MRS Bull.* **2009**, *34*, 504−513.
(18) Yeo, C. C.; Cho, B. J.; Gao, F.; Lee, S. J.; Lee, M. H.; Yu, C. Y.; Liu, C. W.; Tang, L. J.; Lee, T. W. Electron Mobility Enhancement Using Ultrathin Pure Ge on Si Substrate. *IEEE Electron Device Lett.* **2005**, *26*, 761−763.
(19) People, R.; Bean, J. C. Calculation of critical layer thickness versus lattice mismatch for Ge_xSi_{1-x}/Si strained-layer heterostructures. *Appl. Phys. Lett.* **1985**, *47*, 322.
(20) Krishnamohan, T.; Krivokapic, Z.; Uchida, Y.; Nishi, Y.; Saraswat, K. C. Saraswat, High-Mobility Ultrathin Strained Ge MOSFETs on Bulk and SOI With Low Band-to-Band Tunneling Leakage: Experiments. *IEEE Trans. Electron Devices* **2006**, *53*, 990−999.
(21) Fukuda, Y.; Kohama, Y.; Ohmachi, Y. Critical Thickness for the $Si_{1-x}Ge_x$/Si Heterostructure. *Jpn. J. Appl. Phys.* **1990**, *29*, No. L20.
(22) Kuzmin, M.; Lehtiö, J.-P.; Rad, Z. J.; Sorokina, S. V.; Punkkinen, M. P. J.; Laukkanen, P.; Kokko, K. Atomic and electronic structures of Si/Ge(100) interfaces studied by high-resolution photoelectron spectroscopy and scanning tunneling microscopy. *Phys. Rev. B* **2021**, *103*, No. 195312.
(23) Adhikari, H.; McIntyre, P. C.; Sun, S.; Pianetta, P.; Chidsey, C. E. D. Photoemission studies of passivation of germanium nanowires. *Appl. Phys. Lett.* **2005**, *87*, No. 263109.
(24) Chellappan, R. K.; Gajula, D. R.; McNeill, D.; Hughes, G. High temperature thermal stability of the HfO_2/Ge (100) interface as a function of surface preparation studied by synchrotron radiation core level photoemission. *Appl. Surf. Sci.* **2014**, *292*, 345.
(25) Kuzmin, M.; Laukkanen, P.; Punkkinen, M. P. J.; Yasir, M.; Tuominen, M.; Dahl, J.; Lång, J. J. K.; Mäkelä, J.; Kokko, K. Atomic structure and thermally induced transformation of the crystalline BaO/Si(100) junction. *Phys. Rev. B* **2014**, *90*, No. 235405.
(26) Kuzmin, M.; Laukkanen, P.; Yasir, M.; Mäkelä, J.; Tuominen, M.; Dahl, J.; Punkkinen, M. P. J.; Kokko, K.; Hedman, H.-P.; Moon, J.; Punkkinen, R.; Polojärvi, V.; Korpijärvi, V.-M.; Guina, M. Observation of unusual metal-semiconductor interaction and metal-induced gap states at an oxide-semiconductor interface: The case of epitaxial BaO/Ge(100) junction. *Phys. Rev. B* **2015**, *92*, No. 165311.
(27) Kuzmin, M.; Punkkinen, M. P. J.; Laukkanen, P.; Perälä, R. E.; Lång, J. J. K.; Dahl, J.; Adell, J.; Kokko, K. Photoemission and density functional theory study of Ge(100): Clean surface and Yb-induced (2×4) reconstruction. *Surf. Sci.* **2013**, *615*, 88−96.
(28) Tersoff, J.; Hamann, D. R. Theory and Application for the Scanning Tunneling Microscope. *Phys. Rev. Lett.* **1983**, *50*, 1998−2001.
(29) Tersoff, J.; Hamann, D. R. Theory of the scanning tunneling microscope. *Phys. Rev. B* **1985**, *31*, 805−813.
(30) Horcas, I.; Fernández, R.; Gómez-Rodríguez, J. M.; Colchero, J.; Gómez-Herrero, J.; Baro, A. M. WSXM: A software for scanning probe microscopy and a tool for nanotechnology. *Rev. Sci. Instrum.* **2007**, *78*, No. 013705.
(31) Pehlke, E.; Scheffler, M. Evidence for Site-Sensitive Screening of Core Holes at the Si and Ge(001) Surfaces. *Phys. Rev. Lett.* **1993**, *71*, 2338−2341.
(32) Hollinger, G.; Himpsel, F. J. Multiple-bonding configurations for oxygen on silicon surfaces. *Phys. Rev. B* **1983**, *28*, No. 3651.
(33) Oh, J. H.; Yeom, H. W.; Hagimoto, Y.; Ono, K.; Oshima, M.; Hirashita, N.; Nywa, M.; Toriumi, A.; Kakizaki, A. Chemical structure of the ultrathin SiO_2/Si(100) interface: An angle-resolved Si 2p photoemission study. *Phys. Rev. B* **2001**, *63*, No. 205310.
(34) Schmeisser, D.; Schnell, R. D.; Bogen, A.; Himpsel, F. J.; Rieger, D.; Landgren, G.; Morar, J. F. Surface Oxidation States of Germanium. *Surf. Sci.* **1986**, *172*, 455−465.
(35) Kuzmin, M.; Laukkanen, P.; Mäkelä, J.; Yasir, M.; Tuominen, M.; Dahl, J.; Punkkinen, M. P. J.; Kokko, K.; Hedman, H.-P.; Moon, J.; Punkkinen, R.; Lastusaari, M.; Polojärvi, V.; Korpijärvi, V.-M.; Guina, M. Toward the Atomically Abrupt Interfaces of SiO_x/Semiconductor Junctions. *Adv. Mater. Interfaces* **2016**, *3*, No. 1500510.
(36) Prabhakaran, K.; Ogino, T. Oxidation of Ge(100) and Ge(111) surfaces: an UPS and XPS study. *Surf. Sci.* **1995**, *325*, 263−271.
(37) Van Cauwenberghe, O.; Hellman, O. C.; Herbots, N.; Tan, W. J. New SiGe dielectrics grown at room temperature by low-energy ion beam oxidation and nitridation. *Appl. Phys. Lett.* **1991**, *59*, 2031.
(38) Tabet, N. A.; Salim, M. A.; Al-Oteibi, A. L. XPS study of the growth kinetics of thin films obtained by thermal oxidation of germanium substrates. *J. Electron Spectrosc. Relat. Phenom.* **1999**, *101−103*, 233−238.
(39) Pourtois, G.; Houssa, M.; Delabie, A.; Conard, T.; Caymax, M.; Meuris, M.; Heyns, M. M. Ge 3*d* core-level shifts at (100) Ge/Ge(Hf)O_2 interfaces: A first-principles investigation. *Appl. Phys. Lett.* **2008**, *92*, No. 032105.
(40) Molle, A.; Bhuiyan, Md. N. K.; Tallarida, G.; Fanciulli, M. *In situ* chemical and structural investigations of the oxidation of Ge(001) substrates by atomic oxygen. *Appl. Phys. Lett.* **2006**, *89*, No. 083504.
(41) Baldovino, S.; Molle, A.; Fanciulli, M. Influence of the oxidizing species on the Ge dangling bonds at the (100) Ge/GeO_2 interface. *Appl. Phys. Lett.* **2010**, *96*, No. 222110.

(42) Yang, M.; Wu, R. Q.; Chen, Q.; Deng, W. S.; Feng, Y. P.; Chai, J. W.; Pan, J. S.; Wang, S. J. Impact of oxide defects on band offset at GeO_2/Ge interface. *Appl. Phys. Lett.* **2009**, *94*, No. 142903.

(43) Seo, K.-I.; McIntyre, P. C.; Sun, S.; Lee, D.-I.; Pianetta, P.; Saraswat, K. C. Chemical states and electronic structure of a HfO_2/Ge(001) interface. *Appl. Phys. Lett.* **2005**, *87*, No. 042902.

(44) Perego, M.; Scarel, G.; Fanciulli, M.; Fedushkin, I. L.; Skatova, A. A. Fabrication of GeO_2 layers using a divalent Ge precursor. *Appl. Phys. Lett.* **2007**, *90*, No. 162115.

(45) Klesse, W. M.; Scappucci, G.; Capellini, G.; Simmons, M. Y. Preparation of the Ge(001) surface towards fabrication of atomic-scale germanium devices. *Nanotechnology* **2011**, *22*, No. 145604.

(46) Lehtiö, J.-P.; Hadamek, T.; Kuzmin, M.; Laukkanen, P.; Demkov, A. A. Evidence for the Eu 4f Character of Conduction-Band Edge at the Eu_2O_3 Surface Studied by Scanning Tunneling Spectroscopy. *Surf. Sci.* **2021**, *705*, No. 121763.

JACS Au
AN OPEN ACCESS JOURNAL OF THE AMERICAN CHEMICAL SOCIETY
Editor-in-Chief
Prof. Christopher W. Jones
Georgia Institute of Technology, USA
Open for Submissions
pubs.acs.org/jacsau
ACS Publications
Most Trusted. Most Cited. Most Read.

https://doi.org/10.1021/acsmaterialsau.1c00039
ACS Mater. Au XXXX, XXX, XXX−XXX